PROCEEDINGS, 51st Workshop on Geothermal Reservoir Engineering
Stanford University, Stanford, California, February 9-11, 2026
SGP-TR-230

Integrated Diagnostics for Interpreting the Efficiency of the Utah FORGE Enhanced Geothermal System

Smith Leggett[1], Qingwang Yuan[1], Mahmoud Abdellatif[1], Caio Morais De Almeida[1], Rion Nakamoto[1], Queen Nwabueze[1], Hyojeong Seo[1], David Yaw Ofori[1], Dana Jurick[2], Sven Hartvig[3], Peter Rose[4]

1. Bob L. Herd Department of Petroleum Engineering, Texas Tech University
2. Neubrex Energy Services (US), LLC
3. RESMAN Energy Technology
4. Energy and Geoscience Institute, The University of Utah

807 Boston Ave, Lubbock, TX 79409

sleggett@ttu.edu

Keywords: EGS, circulation test, DFOS, fiber optic sensing, chemical tracers, instrumented coiled tubing, spinner flowmeter logging, integrated diagnostics

ABSTRACT

We present results from a one-week circulation test at the Utah FORGE site following the installation of coiled-tubing deployed fiber optic cables in the 16B producer. A comprehensive suite of diagnostics was applied to evaluate flow pathways and reservoir response. A spinner injection log suggested that injection was limited to three heelward stages, while fiber optic distributed sensing revealed three to four primary inflow zones in the producer. Thermal signatures during pressure buildup indicated possible crossflow behavior and provided evidence for a dominant connection point between the wells. Chemical tracer tests, including a freshwater negative tracer test, inform the circulation volume between the wells. We present efforts to use the tracer data to estimate the effective heat exchange area between the wells. Production efficiency increased steadily from 25% to 65% during the test. Bottomhole pressure and temperature measurements provided supporting constraints on reservoir conditions. Collectively, these diagnostics demonstrate the utility of fiber optics and complementary tools for characterizing fluid circulation and reservoir behavior in enhanced geothermal systems.

1. INTRODUCTION

A one-week circulation test was conducted at the Utah FORGE site to characterize the performance of the enhanced geothermal system (EGS) and to support improved forecasting of heat sweep efficiency. The test was designed to replicate, as closely as practical, the conditions of the August 2024 circulation test in order to enable time-lapse comparison of reservoir behavior, while incorporating additional diagnostics and lessons learned from prior operations (McLennan 2024). The experiment was executed under budget and operational constraints consistent with field-scale EGS testing.

The primary objectives of the circulation test were to determine the number of active fracture flow pathways between the injection and production wells, assess the distribution of flow among those pathways, and estimate the effective heat exchange area of the circulating fracture network. These objectives directly relate to understanding short-circuiting, flow uniformity, and overall system efficiency. A secondary objective was to sufficiently recharge the reservoir to support a subsequent injection and flowback test conducted by a separate research team.

To meet these objectives, the circulation test employed an integrated diagnostics approach, combining surface measurements, distributed fiber optic sensing, spinner flowmeter logging, chemical tracer tests, and downhole pressure and temperature measurements. Each diagnostic provides complementary constraints on flow behavior, connectivity, and thermal response, and their combined interpretation enables a more robust assessment of circulation efficiency than any individual measurement.

This paper presents the operational approach, diagnostic methods, and preliminary results from the circulation test, with emphasis on how integrated diagnostics inform interpretation of flow pathways, reservoir connectivity, and production efficiency. Comparisons with results from the 2024 circulation test are used to highlight both persistent and evolving characteristics of the EGS system.

2. METHODS

In this section, we describe the methods used to conduct the circulation test operationally, the diagnostics employed, and interpretation methods applied. Table 1 summarizes similarities and differences between the August 2024 and August 2025 circulation tests.

Table 1: Comparison of the August 2024 and 2025 circulation tests

August 2025 (this work)	August 2024
7 days	30 days
Fiber optic measurements throughout the circulation period	Fiber optic measurements acquired early in the circulation period
Conservative and reversible adsorption tracer tests	Conservative tracer test
Downhole pressure and temperature measurements in 16B	No downhole pressure and temperature measurements
Insulated production and injection temperature measurements	Uninsulated production temperature measurements

2.1 Circulation Operations

Brackish water sourced from well 58B-32 was stored in a 125,000 bbl pit and injected into well 16A at a rate of 10 BPM. A surface choke on the 16B producer was used to maintain sufficient backpressure to ensure single-phase liquid flow in the 16B wellbore. Produced fluids were directed to a sump and then returned to the pit to complete the circulation loop. Figure 1 shows the surface piping and instrumentation used during the test.

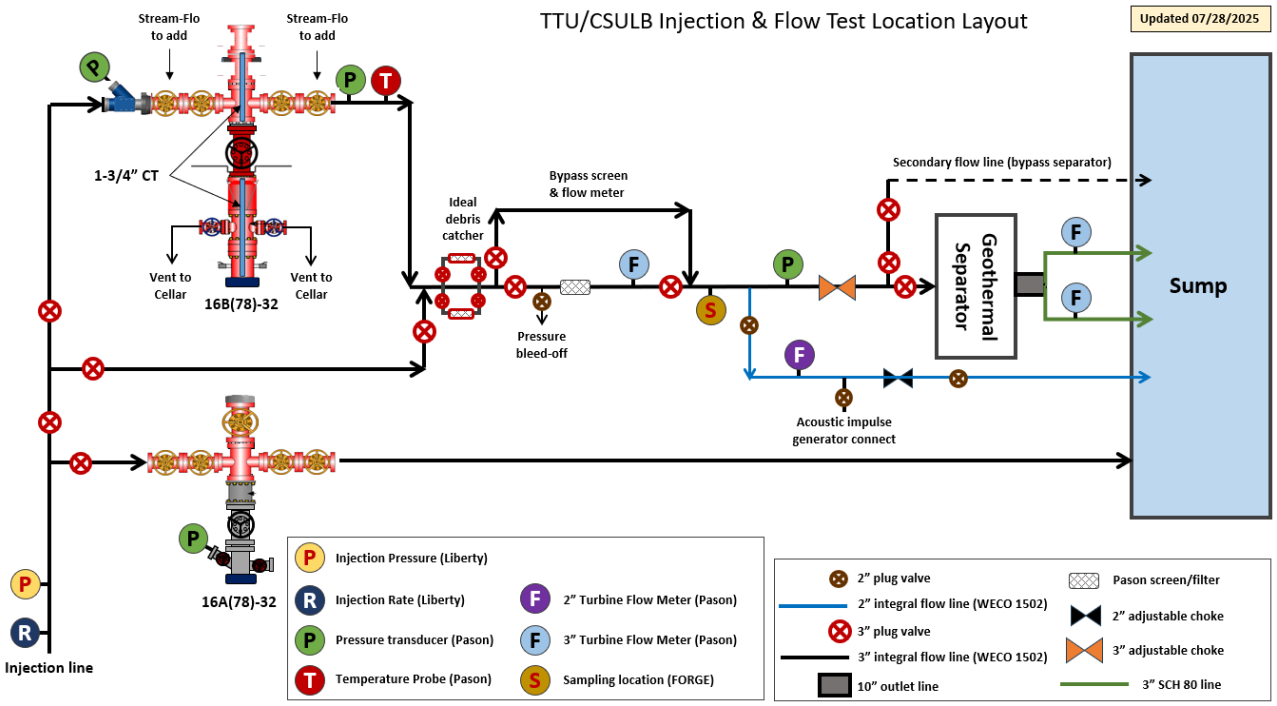

Figure 1: Schematic of the surface piping and instrumentation for the circulation test. The design accommodated a subsequent injection and flowback test.

Injection and production flow rates were monitored using turbine flow meters. Turbine meters located downstream of the geothermal separator were considered unreliable due to two-phase flow, scale production, and sensitivity to liquid level within the separator. All turbine meters were calibrated against the injection flow rate determined from stroke counts of the positive displacement pumps. Production flow rate measurements relied primarily on a 3-inch turbine meter upstream of the choke. Partway through the test, a rattling noise was detected from this meter, and it was temporarily bypassed and replaced.

Most surface measurements were consistent with those used during the August 2024 test, with several additions and modifications. A thermocouple was installed at the suction side of the injection pumps to measure injection fluid temperature (not shown in Figure 1). The thermocouple used to measure production fluid temperature was initially found to be insufficiently immersed in the flow stream, resulting in sensitivity to ambient temperature. Although an extension was added to the probe, ambient effects persisted. Partway through the test, the flowline and tee containing the thermocouple were insulated using a fiberglass blanket, which resulted in a more stable and reliable temperature measurement.

The next two sections describe the fiber optic sensing and chemical tracer methods used during the experiment. In addition to the diagnostics discussed in these sections, a wireline-deployed spinner flowmeter log was run in the 16A well to characterize injection profiles.

2.2 Distributed Fiber Optic Sensing

2.2.1 Instrumented Coiled Tubing String

Fiber optic cables installed external to the 16B production casing failed during circulation testing in August 2024. To enable continued depth-resolved measurements of temperature, acoustic response, strain, and bottomhole pressure and temperature, an instrumented coiled tubing (ICT) string was installed (Leggett et al. 2026). The ICT incorporated two 1/4-inch capillary tubes housing retrievable single-mode (SMF) and multimode (MMF) fiber optic cables for distributed temperature sensing (DTS) and distributed acoustic sensing (DAS), allowing fiber replacement in the event of degradation or failure. An additional capillary tube contained an experimental strain-sensitive fiber designed to enhance strain transfer; however, this fiber failed shortly after installation and is not considered further in this analysis. A tubing-encapsulated conductor (TEC) line provided point measurements of downhole pressure and temperature at the end of the coiled tubing. The ICT was landed at approximately 10,100 ft MD to ensure coverage of all stimulated perforation stages while remaining above the open-hole section to reduce the risk of mechanical sticking as shown in Figure 2. Distributed temperature and acoustic measurements were used to identify inflow locations and relative flow contributions, while pressure and thermal transients constrained reservoir connectivity and circulation efficiency, enabling integrated interpretation of flow pathways and reservoir response during circulation testing.

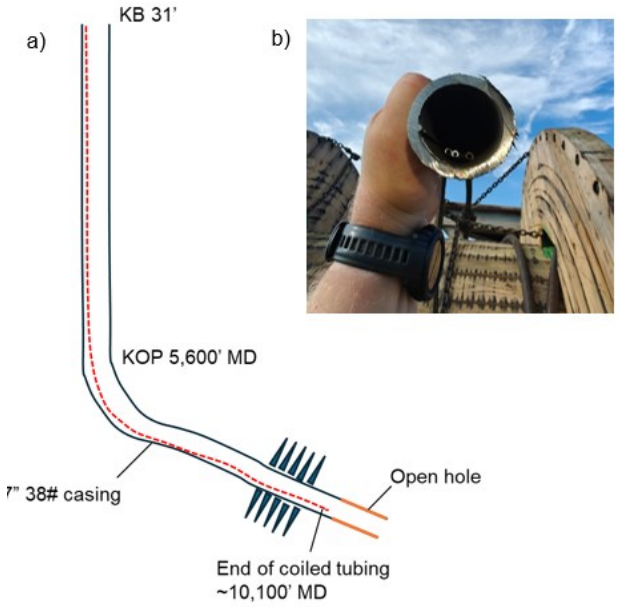

Figure 2: (a) Schematic of the 16B producer showing the instrumented coiled tubing (ICT) landed at ~10,100 ft MD to sense across all perforated intervals while remaining above the open-hole section. (b) Photograph of a cross-section of the coiled tubing showing internal capillary tubes used to house fiber optic cables and instrumentation.

2.2.2 Fiber Optic Sensing Data Acquisition

Neubrex Energy Services acquired and stored all fiber optic sensing data during the circulation experiment. Following the failure of the strain-sensitive fiber, wavelength division multiplexing was used on the retrievable single-mode fiber to simultaneously record distributed acoustic sensing (DAS) and Rayleigh frequency shift distributed strain sensing (RFS-DSS). Distributed temperature sensing (DTS) data were acquired using the multimode fiber.

Depth calibration to the wellhead was performed using a tap test for DAS. For DTS, ice was placed where the fiber-containing capillary tubing exits the wellhead to induce a thermal disturbance. Downhole depths were determined by assuming that the end of the fiber coincided with the end of the coiled tubing string at 10,100 ft MD. Measurements were recorded in a temperature-, humidity-, and vibration-controlled data acquisition trailer.

2.2.3 Production Profiling from Thermal Slugs Tracked by Distributed Fiber Optic Sensing

A complete analysis of the distributed fiber optic sensing dataset is outside the scope of this paper. However, one component of the analysis is included here in which thermally induced slugs are tracked to infer a production profile along the wellbore. Transient temperature anomalies observed in the distributed temperature sensing data were identified and tracked in time and depth, allowing

estimation of thermal slug velocities (Nakamoto and Leggett 2025). The waterfall plot shown in Figure 3a provides an example of thermal slugs observed via RFS-DSS. Figure 3b is obtained by applying temperature change thresholds and performing a linear regression to determine thermal slug velocities for each observed inflow location.

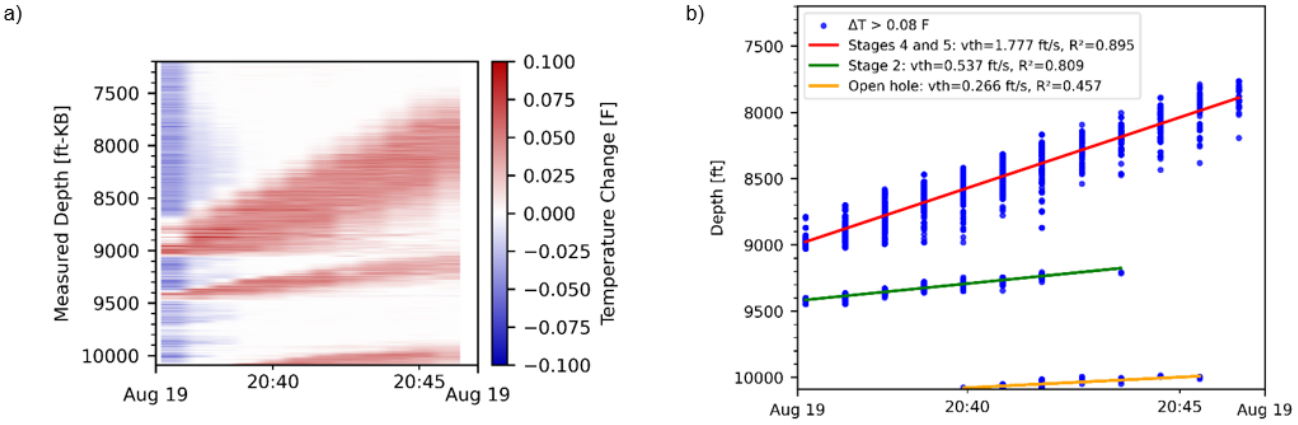

Figure 3: Example of thermal slugs identified with Rayleigh frequency shift based sensing and the extraction of thermal slug velocities from linear fits to temperature change thresholds (Nakamoto and Leggett 2026).

As derived and validated by Nakamoto et al. (2026), the thermal slug velocity can be converted to a bulk fluid velocity from the following equation

$$v_f = \frac{\rho_f c_f A_f + c_s \sum_i W_{s_i}}{\rho_f c_f A_f} v_{th} \quad (1)$$

where v_f and v_{th} are the bulk fluid and thermal slug velocities, ρ is density, c is the specific heat capacity, and A_f is the cross-sectional flow area. The term W_{si} is the mass per unit length of thermally conductive component i (e.g. steel casing, steel coiled tubing string). Subscripts f and s refer to fluid and steel, respectively. Bulk fluid velocity is converted to flow rate by multiplying by the cross-sectional area of the flow stream. Changes in flow rate along the wellbore were then used to allocate production inflow at locations where thermal slugs were observed. Results from this analysis are presented in Section 3.

2.3 Chemical Tracers

Fredd et al. (2025a, 2025b) demonstrated that conservative chemical tracers deployed during EGS circulation tests can be used to estimate the interconnected flow volume of the fracture network at Utah FORGE. Building on this approach, the present study sought to deploy both conservative and reversibly adsorbing tracers in order to constrain not only the circulation volume, but also the effective fracture surface area participating in heat exchange.

Reversibly adsorbing tracers interact with fracture surfaces through weak, reversible sorption processes. As a result, their transport is retarded relative to conservative tracers, with the degree of retardation dependent on the available surface area for sorption. By comparing the breakthrough behavior of conservative and reversibly adsorbing tracers, it is possible to estimate fracture surface area independent of circulation volume (Rose et al. 2025).

Previous tracer experiments at Utah FORGE did not demonstrate reliable reversible adsorption behavior using organic chemical tracers under reservoir conditions (Rose et al. 2025). Inorganic tracers such as lithium and cesium were considered as alternatives; however, background concentrations in the circulating fluid were sufficiently high that achieving a measurable sorption signal would have required injection masses that were cost prohibitive and operationally impractical.

To address these limitations, a reversible adsorption negative tracer test was implemented. Because lithium and cesium were already present at elevated background concentrations in the circulating fluid, freshwater with very low concentrations of these elements was injected to generate a negative tracer signal. In this approach, the recovery of lithium and cesium concentrations toward baseline values reflects reversible sorption and desorption processes occurring at fracture surfaces. Pre-test modeling indicated that injection of approximately 3,000 bbl of freshwater would produce a negative tracer response with sufficient signal-to-noise ratio for subsequent interpretation. Accordingly, approximately 3,000 bbl of Milford City water was delivered to an on-site storage tank and integrated into the injection system. Transfer lines and valving were configured to allow seamless switching between brackish water from the 125,000 bbl pit and freshwater injection without interrupting injection operations.

Table 2 summarizes the tracer injection schedule. The negative tracer test was conducted early in the circulation period to maximize the duration available for sample collection and analysis of reversible adsorption behavior. A second conservative tracer test was conducted

during the spinner flowmeter logging run on Day 5 to satisfy two objectives. First, it enabled direct comparison of tracer response with injection profiles obtained from spinner logging. Second, repeating the conservative tracer test provided a means to assess whether reservoir characteristics had changed between the early negative tracer test and later stages of the circulation experiment, particularly given that the system was far from steady-state conditions early in the test.

Table 2: Tracer injection schedule during the circulation test.

Day	Injection Rate (BPM)	Injected Volume (BBL)	Notes/Other Operations
1	10	14,400	Initial fill of reservoir
2	10	28,800	Co-inject conservative tracer and freshwater (3,000 bbl, 5 hours) for negative tracer test
3	10	43,200	Continue injection
4	10	57,600	Continue injection
5	10	72,000	Conduct 2nd conservative tracer test (1 hour duration) and spinner flowmeter log.
6	10	86,400	Continue injection
7	10	100,800	Continue injection
8	0	100,800	Shut in the wells. Monitor pressure and temperature recovery prior to injection-flowback test.

The next section presents results from the circulation experiment.

3. RESULTS

Preliminary results from the 2025 circulation test at Utah FORGE are presented in this section and compared, where applicable, with observations from the 2024 test. The results integrate surface injection and production measurements, downhole distributed fiber optic diagnostics, spinner flowmeter logging, and chemical tracer data to characterize circulation behavior, reservoir connectivity, and production efficiency. Section 3.1 focuses on surface measurements and distributed sensing observations that describe the temporal evolution of the test and early indicators of flow behavior. Section 3.2 presents injection and production flow profiling results derived from spinner logs and thermal slug tracking. Section 3.3 summarizes preliminary chemical tracer responses, including conservative and negative tracer tests, and their implications for circulation volume and flow partitioning. Collectively, these results provide an integrated perspective on similarities and differences between the 2024 and 2025 circulation tests.

3.1 Surface Measurements

This section presents and provides preliminary interpretation of surface injection and production measurements acquired during the circulation test. Figure 4 shows injection and production pressures and flow rates measured during the seven-day circulation period, followed by a one-day shut-in. The injection rate was held nearly constant throughout the test, while injection pressure exhibited a slight downward trend. Short-duration drops in injection pressure correspond to temporary operational interruptions, including pump outages, replacement of a leaking valve on the production flowback line, and wireline rig-up for spinner flowmeter logging.

Early in the test, the 16B producer was shut in while injection continued in 16A to promote reservoir pressure recharge. Recharge was inferred from the observed pressure buildup at the 16B wellhead during the shut-in period. Reopening criteria were defined as either 24 hours of shut-in or a pressure buildup of 1,000 psi. As the pressure approached the 1,000 psi threshold near the onset of nighttime operations, the choke was reopened to mitigate the risk of exceeding operational criteria during the night shift. Following reopening, the production rate increased steadily over the remainder of the circulation period but remained below the injection rate of 10 BPM, reaching a maximum of approximately 6.5 BPM near the end of Day 7. Steady-state production conditions were not achieved. At the conclusion of the circulation period, injection and production operations were shut down; measurements continued during a one-day shut-in before subsequent injection-flowback operations.

Production pressure was controlled using a surface choke to maintain single-phase liquid flow. Discontinuities in the 16B surface pressure record coincide with incremental choke openings. Each adjustment resulted in a rapid pressure decrease followed by a gradual pressure recovery, consistent with continued reservoir recharge.

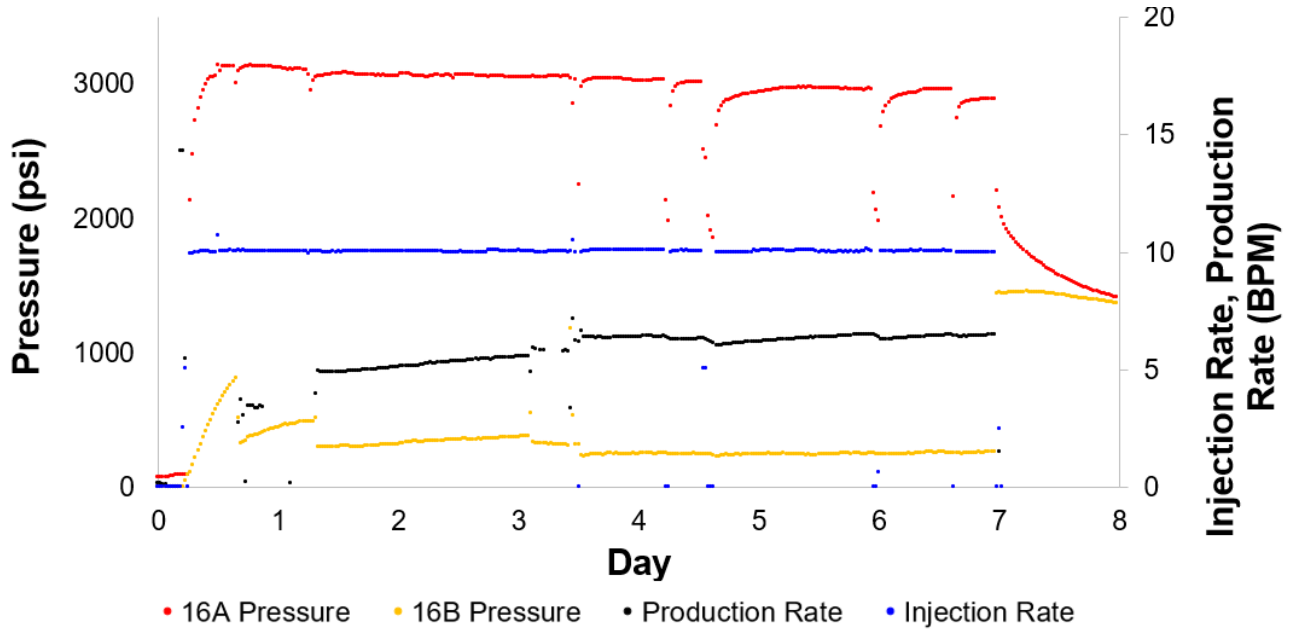

Figure 4: Injection and production pressures and rates during the circulation test.

Figure 5 shows the evolution of production efficiency during the circulation test, compared with results from 2024. Rather than time, the horizontal axis represents the cumulative volume stored in the system, defined as the difference between injected and produced volumes. Before discussing trends in this plot, it is important to address the reliability and sources of uncertainty associated with the computed efficiencies.

During the 2025 test, production rates reported in Figure 4 were measured using a turbine flowmeter located upstream of the choke, which is considered to provide relatively reliable measurements under single-phase liquid flow conditions. In contrast, investigators reported erratic behavior from a flowmeter installed in the same location during the 2024 test, and those measurements were deemed unreliable. As a result, production efficiency for both years shown in Figure 5 was calculated using production flow rates measured downstream of the geothermal separator to ensure an apples-to-apples comparison.

Uncertainty exists in these downstream measurements. Scale intermittently released from the geothermal separator could enter the liquid dump lines and partially obstruct the turbine flowmeters. In addition, flashing downstream of the separator can result in two-phase flow through the meters, further degrading measurement accuracy. No flash calculations were performed to account for steam generation in the efficiency estimates.

With these limitations in mind, production efficiency exhibits similar initial values in both the 2024 and 2025 tests, although the parameter is noisy. During the 2025 circulation test, volumetric production efficiency increased steadily from approximately 25% to 65%. When compared to the 2024 test, the data suggest slightly lower overall efficiency in 2025; however, it remains unclear whether this difference is significant given the measurement uncertainties described above.

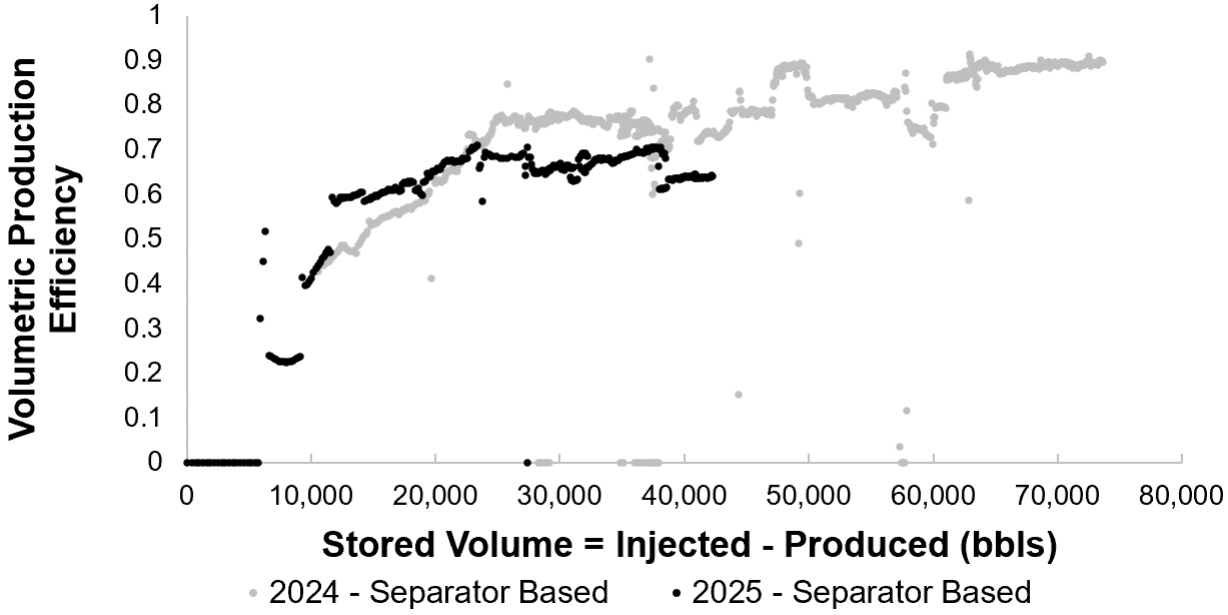

Figure 5: Production volumetric efficiency in 2024 (gray) and 2025 (black) circulation tests based on flow rate measurements from turbine flowmeters downstream of the geothermal separator.

Figure 6 compares produced fluid temperatures from the August 2025 circulation test with the uninsulated ("raw") temperature measurements acquired during the August 2024 test. During the 2025 test, the thermocouple was insulated after approximately 25,000 bbl of injection, resulting in a clear increase in measured temperature and a reduction in signal noise. The produced fluid temperature measured in 2025 is slightly higher than in 2024, likely due to the improved thermal insulation. As observed in 2024, the produced temperature in 2025 exhibits a gradual upward trend over the course of the test.

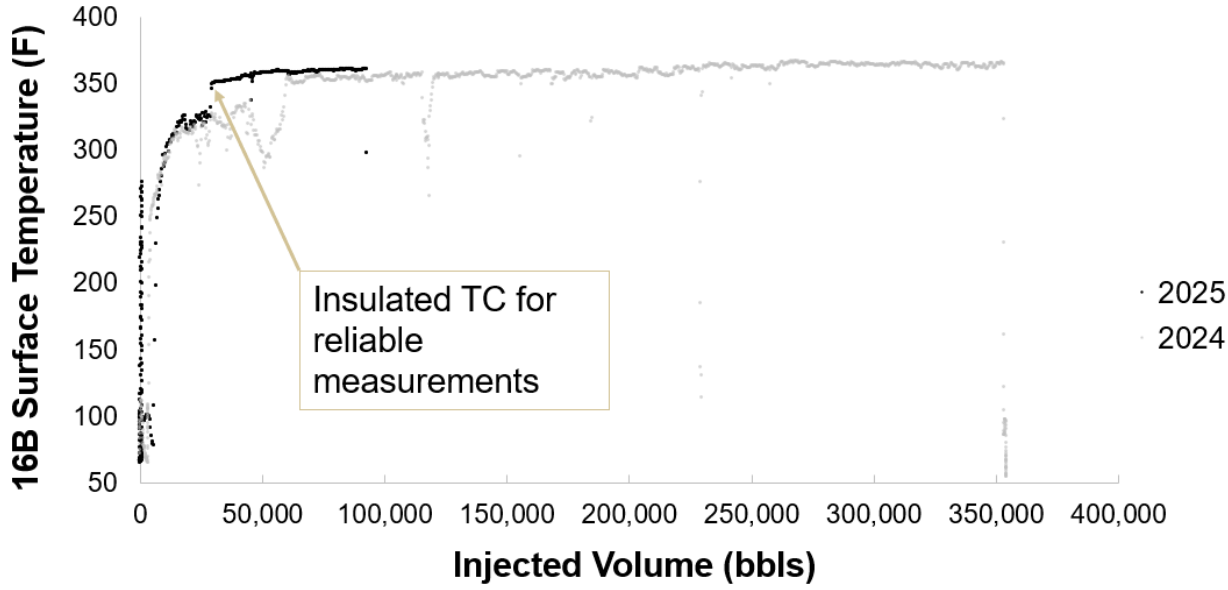

Figure 6: Production temperature in August 2024 (gray) and August 2025 (black) circulation tests.

Distributed fiber optic measurements afforded a unique observation at the beginning of the circulation test, during injection into the 16A while the 16B producer remained shut-in. Cooling signals were observed propagating from shallow perforated intervals toward the open-hole section of 16B, as shown in Figure 7. These thermal slugs are interpreted as evidence of crossflow within the wellbore, indicating that more conductive flow pathways connect the fracture network to the perforated intervals than to the open-hole section. Under these conditions, the reservoir surrounding the open hole appears to be recharged by fluid migrating through the fracture network into the upper perforations of 16B and exiting through the open-hole section.

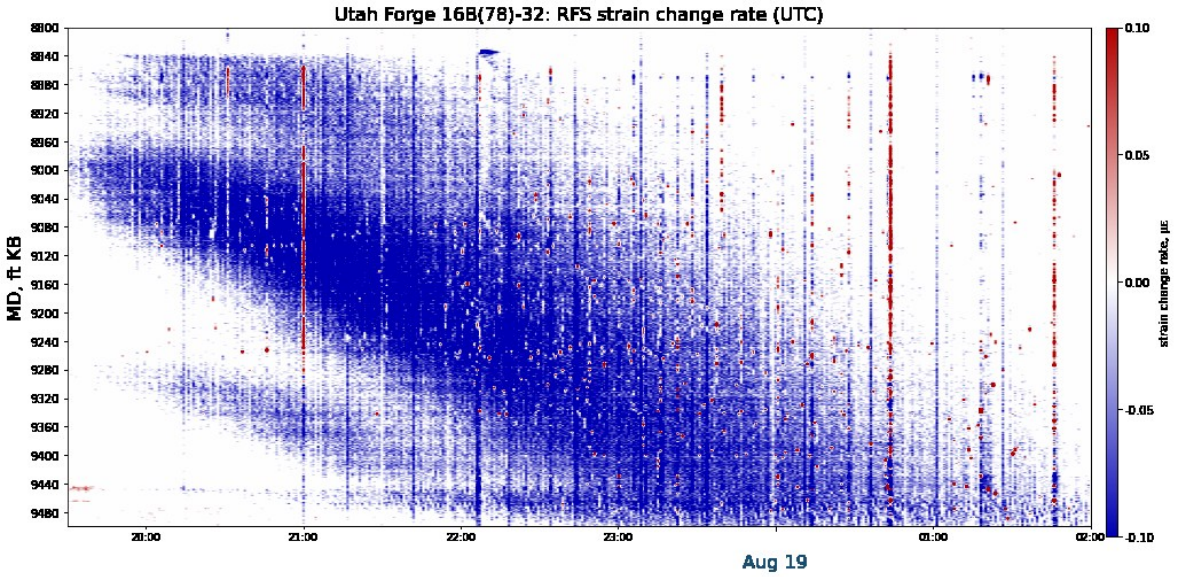

Figure 7: Rayleigh frequency shift–derived temperature changes showing thermal slugs propagating toward the open-hole section of 16B during initial injection into 16A while 16B remained shut in, interpreted as crossflow within the wellbore.

3.2 Injection and Production Flow Profiling

Spinner flowmeter-derived injection profiles in the 16A well from the August 2024 and August 2025 circulation tests are compared in Figure 8. Injection into Stage 5 is similar between the two tests; however, substantial differences are observed in other stages. In the 2025 results, injection is primarily limited to three heelward stages, whereas injection was more distributed across stages in 2024. Stage 10 dominates the 2025 injection profile, accounting for nearly 50% of the total injected flow, while injection into stages below Stage 4 is markedly reduced. In addition, the relative injection rates between Stages 8 and 9 appear to have reversed between 2024 and 2025. As this comparison is preliminary, potential causes for these changes are not evaluated here.

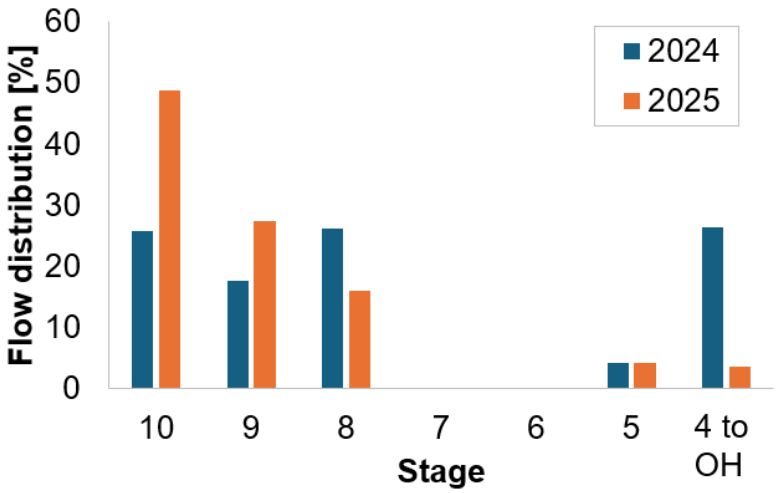

Figure 8: Injection profiles obtained from spinner flowmeter wireline logs acquired during the August 2024 (blue) and August 2025 (orange) circulation tests.

In contrast to the injection profiles, production allocations appear broadly consistent between the August 2024 and August 2025 tests (Table 3). As shown in Figure 3, induced thermal transients propagate from four zones at the stage level. Individual clusters are not resolved. At a high level, approximately one-third of the produced fluid originates from the open-hole section through Stage 3 in both datasets, while roughly two-thirds is produced from Stages 4 and 5. In the 2025 analysis, production profiles were derived from thermal slug tracking using distributed fiber optic sensing; these preliminary results do not permit delineation of inflow between Stages 4 and 5,

and are therefore reported in aggregate. In comparison, the 2024 spinner flowmeter log did not extend below Stage 4, and production from the open-hole section through Stage 3 is similarly aggregated. Despite these limitations, the thermal slug analysis indicates that production is not evenly distributed across the open-hole and upper stages. Preliminary results suggest little to no inflow from Stages 1 and 3, a 23% contribution from Stage 2, and a moderate contribution of approximately 9% from the open-hole section.

Table 3: Production profiles determined from a spinner flowmeter wireline log acquired in August 2024 and from thermal slug tracking using distributed fiber optic sensing during the August 2025 circulation test.

Completion Stage	Spinner Log (2024)	Thermal Slug (2025)
Open Hole	36%	9%
1		0%
2		23%
3		0%
4	38%	68%
5	26%	

3.3 Preliminary Chemical Tracer Results

Preliminary results from two chemical tracer pulses are presented below. The first tracer pulse, conducted on Day 2 of operations, consisted of a conservative tracer co-injected with approximately 3,000 bbl of freshwater to generate a negative tracer signal. Results from this test are shown in Figure 9. A second conservative tracer pulse, co-injected with approximately 600 bbl of brackish water, was conducted on Day 5, with results shown in Figure 10.

For Tracer Test 1, a decrease in lithium concentration relative to background levels is observed, confirming the successful introduction of the freshwater pulse. For a reversibly adsorbing tracer, a delayed breakthrough peak, or in the case of a negative tracer a delayed concentration minimum, would be expected relative to the conservative tracer. However, the lithium response appears to coincide with the conservative tracer (RWT-1201), suggesting little to no observable retardation within the resolution of the current dataset. The lithium concentration curve shown in Figure 9 is incomplete, as additional samples are still being processed. Cesium analysis has not yet been completed. As a result, further analysis is required to assess whether reversible adsorption behavior is present and, if so, to estimate the effective fracture surface area. At a minimum, these preliminary results demonstrate that chloride (response not shown but similar to lithium) or other conservative ions can serve as effective tracers in a negative tracer framework, providing an alternative to organic chemical tracers.

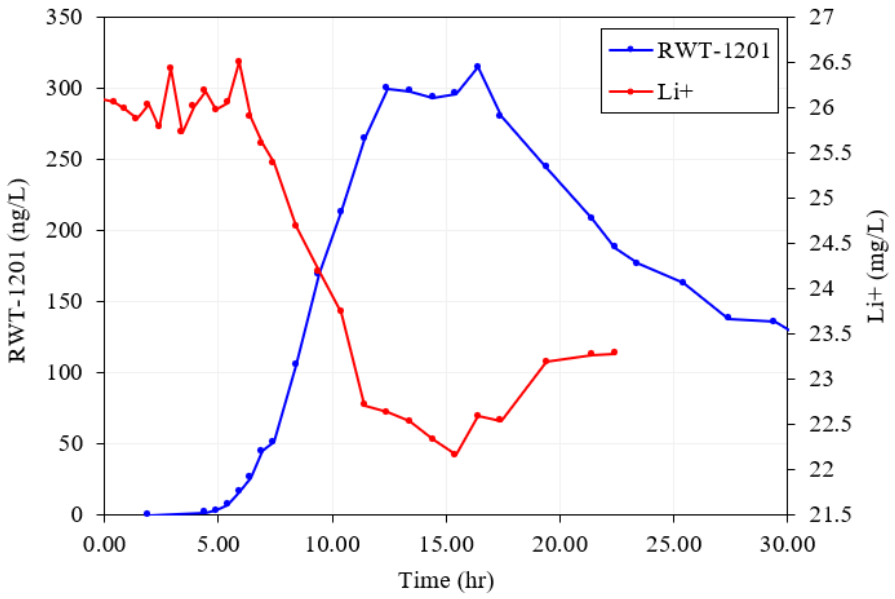

Figure 9: Comparison of conservative tracer pulse #1 (RWT-1201) and lithium concentration during the freshwater negative tracer test. Lithium data processing is ongoing, and the curve shown here is incomplete.

Results from Tracer Test 2, shown in Figure 10, present the response of a conservative tracer pulse injected on Day 5. A semi-analytical transport model was applied to interpret the tracer breakthrough behavior. The tracer response is well represented by a two-component flowing system, consisting of one highly conductive pathway with an estimated circulation volume of approximately 5,000 bbl and a second pathway with a circulation volume of approximately 8,000 bbl. This two-component behavior is consistent with interpretations reported by Fredd et al. (2025a, 2025b) for tracer tests conducted at Utah FORGE in 2024 .

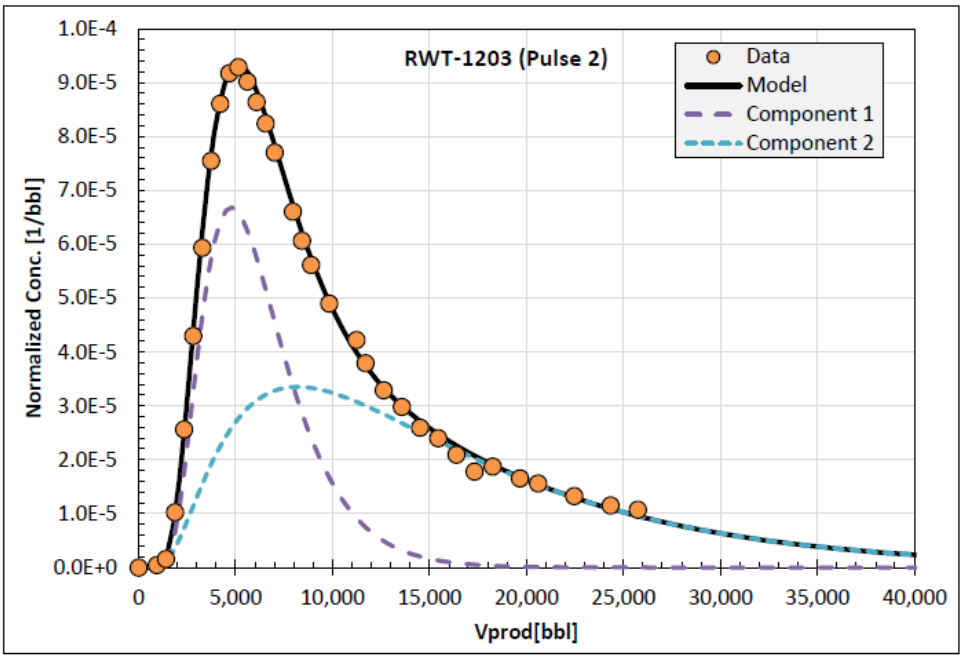

Figure 10: Breakthrough response of conservative tracer pulse #2 and corresponding semi-analytical transport model fit, indicating two dominant flowing components.

CONCLUSIONS

Results from the 2024 and 2025 circulation tests at Utah FORGE exhibit both similarities and key differences that are best understood through an integrated diagnostics framework. Injection profiles are broadly comparable between the two tests; however, the 2025 test shows increased injection into Stage 10 and reduced contribution from the open-hole section relative to 2024. In contrast, production profiles appear largely consistent between the two years, suggesting that dominant production pathways remained stable despite changes in injection distribution.

Chemical tracer results further support this interpretation. Conservative tracer responses from 2024 and 2025 are similar, indicating comparable effective circulation volumes between tests. Preliminary results from the 2025 negative tracer experiment demonstrate that freshwater injection can act as a viable tracer pulse when background concentrations of inorganic tracers are high, providing a practical alternative to traditional chemical tracer deployments. While reversible adsorption behavior has not yet been clearly resolved, the approach shows promise for future estimation of effective fracture surface area.

Thermal and fiber optic measurements provide additional insight into reservoir connectivity and flow behavior that is not apparent from surface data alone. Distributed sensing revealed crossflow within the 16B well while it was shut in, indicating weaker hydraulic connection between 16A and the open-hole section of 16B relative to the perforated intervals. In 2025, the produced fluid temperature was slightly higher than in 2024, although this difference is likely attributable to measurement uncertainty associated with the absence of thermocouple insulation in 2024. Overall production efficiency was lower in 2025; however, uncertainty in flow rate measurements may also contribute to this apparent difference.

Collectively, these results demonstrate that integrated diagnostics combining surface measurements, distributed fiber optic sensing, spinner logging, and chemical tracers provide a more complete and defensible interpretation of EGS circulation behavior than any single diagnostic alone. This integrated approach is particularly valuable for identifying flow partitioning, transient crossflow behavior, and uncertainties in efficiency estimates, and it offers a practical framework for future Utah FORGE circulation and flowback experiments.

ACKNOWLEDGEMENTS

This material is based upon work supported by the Department of Energy, Office of Energy Efficiency and Renewable Energy (EERE), under Award Number DEEE0007080.

In addition, the authors would like to acknowledge the support of the Utah FORGE team in planning and executing the experiment, including but not limited to: John McClennan, Kevin England, and Leroy Swearingen. We would also like to acknowledge Matthew Becker and the CSULB team for collaboration and joint planning of the project.

REFERENCES

Fredd, C.N.; De Cerf, C.K.; Giri, P.; Hartvig, S.K.; Huseby, O.; McLennan, J.; England, K.: "Advanced Tracer Interpretation at Utah FORGE Provides New Insights on Completion and Stimulation Challenges for Enhanced Geothermal Systems and Tight Formations", paper URTeC 4258944 presented at the Unconventional Resources Technology Conference held in Houston, Texas, USA, 9-11 June 2025

Fredd, C.N.; Giri, P.; Hartvig, S.K.; Huseby, O.; McLennan, J.; England, K.: " New Insights into Flow Path Characteristics at Utah FORGE Unlock Opportunities for Optimizing Enhanced Geothermal Systems", paper GRC Transactions, Vol. 49, 2025. presented at the Geothermal Rising Conference held in Reno, Nevada, USA, 26-29 October 2025

Leggett, Smith, Keough, Dan, Andriianov, Aleksei, Rampurawala, Murtaza, and Jurick, Dana. 2026. Deploying Coiled Tubing Conveyed Fiber Optic Cables at the Utah FORGE Enhanced Geothermal System. *Proc.,* Proceedings of the 51st Workshop on Geothermal Reservoir Engineering, Stanford, CA, 2026/02/09.

McLennan, John. 2024. *Utah FORGE: Wells 16A(78)-32 and 16B(78)-32 Extended Circulation Test Data - August and September 2024*, Energy and Geoscience Institute at the University of Utah (Reprint). https://doi.org/10.15121/2475065.

Nakamoto, Rion and Leggett, Smith. 2025. Development of a Transient Wellbore Heat Transfer Model Validated with Distributed Temperature Sensing Data. *Sensors* **25** (21): 6583. https://www.mdpi.com/1424-8220/25/21/6583.

Nakamoto, Rion, Leggett, Smith 2026. An Analytical Approach to Production Logging in Enhanced Geothermal Systems Using Distributed Fiber Optic Thermal Slug Tracking. Geothermics. Under review.

Rose, Peter E., Abdellatif, Mahmoud, Yuan, Qingwang, and Leggett, Smith. 2025. The Use of Reversibly Adsorbing Tracers for Characterizing Reservoir Fracture Surface Area in Engineered Geothermal Systems. *Proc.,* Proceedings of the 50th Workshop on Geothermal Reservoir Engineering, Stanford, CA, 2025/02/10.